Molecular Logic Gates

Deutsche Ausgabe: DOI: 10.1002/ange.201504584
Internationale Ausgabe: DOI: 10.1002/anie.201504584

A Molecular Platform for Multistate Near-Infrared Electrochromism and Flip-Flop, Flip-Flap-Flop, and Ternary Memory**

*Bin-Bin Cui, Jian-Hong Tang, Jiannian Yao, and Yu-Wu Zhong**

Abstract: *A diruthenium complex with a redox-active amine bridge has been designed, synthesized, and studied by single-crystal X-ray analysis and DFT and TDDFT calculations. It shows three well-separated redox processes with exclusive near-infrared (NIR) absorbance at each redox state. The electropolymerized film of a related vinyl-functionalized complex displays multistate NIR electrochromism with low operational potential, good contrast ratio, and long retention time. Flip-flop, flip-flap-flop, and ternary memories have been realized by using the obtained film (ca. 15–20 nm thick) with three electrochemical inputs and three NIR optical outputs that each displays three levels of signal intensity.*

The use of molecules or molecular assemblies for information processing is one attractive perspective of molecular science. Since the pioneering work of de Silva in 1993,[1] a large number of molecular logic gates have been demonstrated.[2–4] Among them, sequential molecular logics with input-history-dependent outputs are very useful for memory devices. A typical example is set/reset flip-flop[5,6] built from a pair of cross-coupled NOR logic gates or a ternary flip-flap-flop memory.[7] A ternary (or higher) memory system has the advantage of a higher information density with respect to a binary system,[7–9] which is critical to meet the challenge of information storage.

A truly ternary memory needs three inputs and three outputs with three signal levels. However, molecular materials displaying such functions are very scarce. This contrasts with a previously reported system built from bistable materials coupled with an additional intermediate mixed-valent state or with a single output showing three levels of signal intensity.[7] In addition to the material issue, it is essential to transform the solution-phase demonstrations to solid support for eventual practical applications.[10–13] This could be realized by depositing the materials in the form of monolayers,[5,9,14–19] multilayers,[7,20–23] or polymeric thin films.[24–28] We report here an unprecedented redox-active system that mimics the surface-confined flip-flop and truly flip-flap-flop or ternary memory.

The basic molecular material is a new diruthenium complex $\mathbf{1}(PF_6)_2$ (Figure 1 a). This compound was designed by taking the following considerations. The two cyclometalated ruthenium complexes are connected to a redox-active amine bridge at the *para* position of the Ru–C bond, which is believed to allow a strong electronic coupling among the [Ru–N–Ru] array.[29] As a result, multiple redox states can be accessed at low electrochemical potentials and each state can be distinguished by strong near-infrared (NIR) charge transfer absorptions. The use of electrical inputs is compatible with existing electronic technologies. The use of redox-active molecules for electrochemical logic gates and information storage has been known.[13–19,30–32] The use of NIR absorption signals as the outputs has the advantages of being low-energy, non-destructive, and low-interference with substrates.[33–36] NIR electrochromic materials are potentially useful as variable optical attenuators in fiber telecommunications.[37,38] After attaching suitable functional groups, this complex can be deposited onto electrode surfaces using suitable thin-film-formation methods.[19,26,30] Thin films of cyclometalated ruthenium complexes have been known to have long reten-

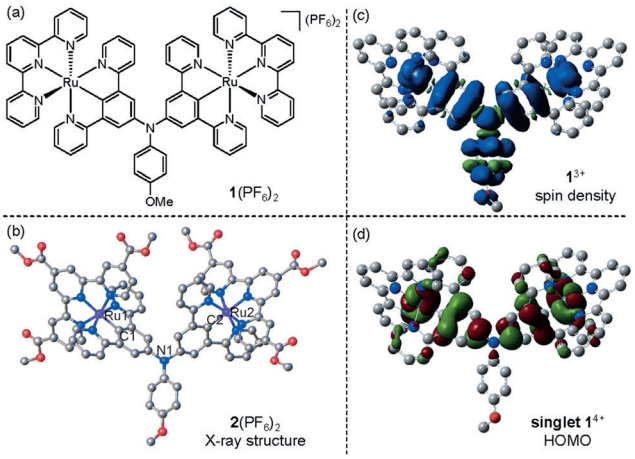

Figure 1. a) Chemical structure of $\mathbf{1}(PF_6)_2$. b) Thermal ellipsoid plot of the single-crystal structure of $\mathbf{2}(PF_6)_2$ at 30% probability. Hydrogen atoms and anions are omitted. Atom color code: C grey; N blue; Ru magenta. Selected bond length: Ru1–C1 1.97 Å; Ru2–C2 1.93 Å; Ru1–N1 6.18 Å; Ru2–N1 6.21 Å; Ru1–Ru2 9.94 Å. c) DFT-calculated spin density distribution of $\mathbf{1}^{3+}$. d) The isodensity plot of the HOMO of singlet $\mathbf{1}^{4+}$.

[*] B.-B. Cui,[+] J.-H. Tang,[+] Prof. J. Yao, Prof. Y.-W. Zhong
Beijing National Laboratory for Molecular Sciences
CAS Key Laboratory of Photochemistry
Institute of Chemistry, Chinese Academy of Sciences
Beijing 100190 (P.R. China)
E-mail: zhongyuwu@iccas.ac.cn

[+] These authors contributed equally to this work.

[**] We thank the National Natural Science Foundation of China (grants 91227104, 21271176, 21472196, and 21221002), the National Basic Research 973 program of China (grant 2011CB932301), the Ministry of Science and Technology of China (grant 2012YQ120060), and the Strategic Priority Research Program of the Chinese Academy of Sciences (grant XDB 12010400) for support.

Supporting information for this article is available on the WWW under http://dx.doi.org/10.1002/anie.201504584.

tion time because of the good stability of each redox state,[19,25] which is important for their uses as memory materials.

The synthesis and characterization of $\mathbf{1}(PF_6)_2$ are given in the Supporting Information (SI). Simply speaking, it is synthesized from the reaction of [Ru(tpy)Cl_3] (tpy is the terminal ligand 2,2′:6′,2″-terpyridine) with the central bridging ligand. This complex has been fully characterized by obtaining an NMR spectrum, a MALDI-TOF mass spectrum with consistent isotope distribution, and by microanalysis. We failed to obtain a single crystal of this complex. However, a related complex $\mathbf{2}(PF_6)_2$ with the same bridging ligand albeit different terminal ligands, namely trimethyl-4,4′,4″-tricarboxylate-2,2′:6′,2″-terpyridine, has also been synthesized, which fortunately yielded a single crystal suitable for X-ray diffraction analysis (Figure 1b). The central triarylamine bridge has a three-wheel-propeller geometry. Each ruthenium ion has a distorted octahedral configuration with two planar tridentate ligands. The two NCN ligands have a torsion angle of 115.38° with respect to the central N atom. The Ru–C bonds (shorter than 2.0 Å) are slightly shorter with respect to Ru–N bonds (2.01–2.10 Å).

Figure 2 shows the anodic cyclic voltammograms (CV) and differential pulse voltammograms (DPV) of $\mathbf{1}(PF_6)_2$. Three consecutive redox couples at +0.21, +0.44, and +1.03 V versus Ag/AgCl are observed. The wide separation between each two neighboring waves ensures the good thermodynamic stability and ready accessibility of four different redox states A, B, C, and D.

To characterize the absorption spectra of $\mathbf{1}(PF_6)_2$ at different redox states, it was stepwisely oxidized by electrolysis at a transparent indium-tin-oxide (ITO) glass electrode and the NIR absorption spectral changes were recorded (Figure 3). When the potential was gradually applied from 0.01 V to +0.40 V versus Ag/AgCl, a distinct absorption band centered on 1680 nm appeared. When the potential was further increased from +0.40 V to +0.80 V, the NIR band at 1680 nm gradually decreased and a new peak at 1170 nm appeared. In a third step oxidation (from +0.80 V to +1.20 V), the new peak at 1170 nm decreased again and the appearance of a band at 750 nm was observed. These three-step spectral changes are fully reversible when the potential was decreased from +1.20 V to 0.01 V. The applied potentials correlate well with the single, double, and triple oxidations shown in Figure 2. The absorptions in the visible region

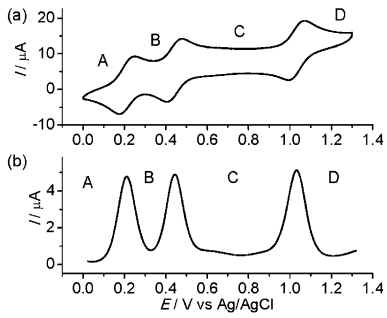

Figure 2. Anodic a) CV and b) DPV of $\mathbf{1}(PF_6)_2$ in 0.1 M Bu_4NClO_4/CH_3CN.

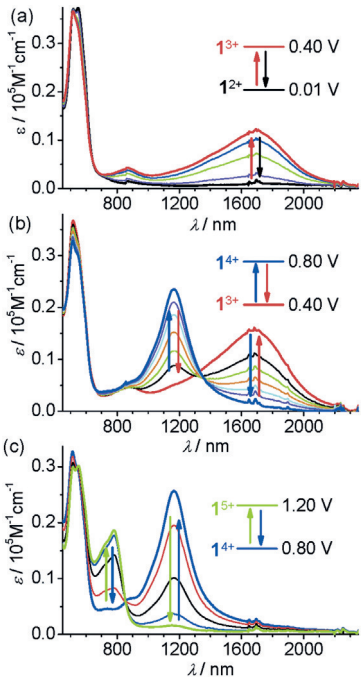

Figure 3. Absorption spectral changes of $\mathbf{1}(PF_6)_2$ upon a) single, b) double, and c) triple oxidation by electrolysis with an ITO glass electrode in 0.1 M Bu_4NClO_4/CH_3CN. The applied potentials were referenced versus Ag/AgCl.

decreased a little in all three step processes. In this way, the four redox states of complex **1** can be distinguished by the NIR absorption spectra. More importantly, each of the three higher redox states is characterized by an exclusive and well-separated absorption peak (1680 nm for $\mathbf{1}^{3+}$; 1170 nm for $\mathbf{1}^{4+}$; 750 nm for $\mathbf{1}^{5+}$) and these states can be simply triggered by well-separated electrochemical potentials. This feature will make it perfectly useful in flip-flop and flip-flap-flop devices.

The structure of the singly oxidized state $\mathbf{1}^{3+}$ has been optimized with B3LYP/LANL2DZ/6-31G*/CPCM(CH_3CN) (see details in the SI). The spin density (α-β) is delocalized across the whole [Ru–N–Ru] segment (Figure 1c). The two ruthenium ions and the central nitrogen atom have contributions of 0.157, 0.144, and 0.239, respectively. The two cyclometalating phenyl rings and 4-methoxy phenyl ring have contributions of 0.175, 0.164, and 0.113, respectively. According to the TDDFT results, the NIR absorptions of $\mathbf{1}^{3+}$ are largely due to the β spin transition from the highest occupied spin orbital (HOSO) to the lowest unoccupied spin orbital (LUSO) (the D_1 excitation, Table S1 and Figure S1), which could be considered as the charge transfer from two ruthenium components to the middle triarylamine unit.

For the doubly oxidized form $\mathbf{1}^{4+}$, there are two possible spin states (singlet and triplet) depending on the spin directions. The singlet state was calculated to be 0.11 eV lower in energy relative to the triplet state. The highest occupied molecular orbital (HOMO) of singlet $\mathbf{1}^{4+}$ is dominated by two ruthenium components (Figure 1d). Figure S2 shows the spin-density population of triplet $\mathbf{1}^{4+}$, which is also dominated by two ruthenium components. The TDDFT results in the singlet state show that the NIR absorption of

$\mathbf{1}^{4+}$ is mainly attributed to the electronic transition from the HOMO to the lowest unoccupied molecular orbital (LUMO) (the S_5 excitation, Table S2 and Figures S3 and S4). For the triply oxidized form $\mathbf{1}^{5+}$, the absorption at 750 nm is characteristic for triaryl aminium radical cations.[39,40]

To demonstrate the utility of complex **1** in surface-confined molecular gates and memories, we first considered to prepare thin films of related complexes by electropolymerization.[24,26,41,42] Electropolymerized films are adhesive and thickness-controllable. The coordination environments can be fully retained. The reaction of the same central bridging ligand with [Ru(vtpy)Cl_3] (vtpy is 4′-vinyl-2,2′:6′,2″-terpyridine) gave the vinyl-terminated diruthenium complex $\mathbf{3}(PF_6)_4$ (Figure 4a). This complex was isolated as the doubly oxidized form, as characterized by MALDI-TOF mass spectrometry, microanalysis data, and absorption spectroscopy (Figure S5).

The reductive electropolymerization[26,42] of $\mathbf{3}(PF_6)_4$ proceeded smoothly on indium-tin-oxide (ITO) surfaces to give adhesive poly-$\mathbf{3}^{n+}$ films, as evidenced by the continuous increase of the current during the repeated cathodic cyclic voltammetric scans (Figure 4c). The obtained film displays similar three redox couples in clean electrolyte solution as has been observed for $\mathbf{1}(PF_6)_2$. Both anodic and cathodic currents are linearly dependent on the scan rate (Figure S6), which is characteristic of redox events confined on electrode surfaces. The surface coverage Γ (determined by the charge under the electrochemical waves) can be easily varied by changing the duration of electropolymerization (Figure 4d).

The above obtained polymeric film adheres to the ITO substrate tightly, as can be seen from SEM pictures taken from the cross section of the film (Figure S7). Judging from the SEM picture, a film with Γ of 2.6×10^{-9} mol cm^{-2} is about 40 nm thick. Figure 4b shows the typical AFM surface morphology of the poly-$\mathbf{3}^{n+}$/ITO film with a root mean square (rms) of 3.1 nm. The thickness estimated by measuring the step height produced by scanning across a scratching edge is about 120 nm for a film of 1.0×10^{-8} mol cm^{-2} (Figure S8). The SEM and AFM pictures consistently suggest that the film thickness can be estimated by the surface coverage (a surface coverage of 1.0×10^{-10} mol cm^{-2} corresponds to 1.2–1.5 nm film thickness). The counter anions of poly-$\mathbf{3}^{n+}$ are mainly ClO_4^- anions (instead of PF_6^-) incorporated from the electrolyte ($n$$Bu_4NClO_4$) during electropolymerization. This is supported by FTIR data (Figure S9). The X-ray photoelectron spectrum (XPS) of the film evidences the Ru3d5 signal at 282.62 eV with the C/N/O/Cl/Ru/atomic ratio of 67.44/6.6/17.15/1.63/0.57 (Figure S10 and Table S3).

Upon stepwise oxidation from poly-$\mathbf{3}^{2+}$ through poly-$\mathbf{3}^{5+}$, the ITO film shows similar three-step spectral changes as have been observed for $\mathbf{1}(PF_6)_2$ in solution (Figure S11). Figure 4e shows the absorption spectra and film pictures of poly-$\mathbf{3}^{n+}$ at different redox states. The difference of the absorption spectrum in the visible region of poly-$\mathbf{3}^{2+}$, poly-$\mathbf{3}^{3+}$, and poly-$\mathbf{3}^{4+}$ is not big. The color change of the film at these states is small (magenta, chocolate, violet red, respectively). The film at the poly-$\mathbf{3}^{5+}$ state is light blue. A relatively thick film ($\Gamma=1.0\times10^{-8}$ mol cm^{-2}) shows good contrast ratio (ΔT%) upon repeated electrochromic switching (42% at 1680 nm; 57% at 1170 nm; 44% at 750 nm; Figure S12). It should be pointed out that these performances are among the best contrast ratios ever achieved for NIR electrochromism.[25,37,38,42–45]

Two important features of the above films are important for their uses in flip-flop and flip-flap-flop memories. One is that poly-$\mathbf{3}^{3+}$, poly-$\mathbf{3}^{4+}$, and poly-$\mathbf{3}^{5+}$ possess exclusive input and output signals. Another is that each output signal has a long retention time (Figure S13). The poly-$\mathbf{3}^{3+}$ state is essentially a stable state. The absorption at 1680 nm only

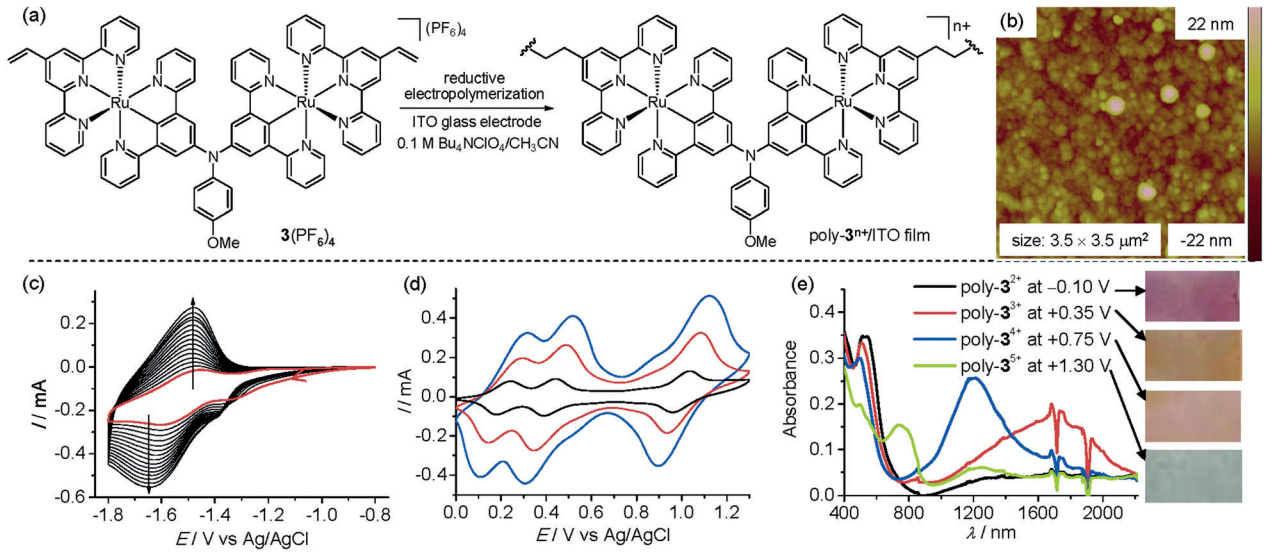

Figure 4. a) Schematic representation for the reductive electropolymerization of $\mathbf{3}(PF_6)_4$. b) AFM height image of the obtained poly-$\mathbf{3}^{n+}$/ITO film ($\Gamma=1.0\times10^{-8}$ mol cm^{-2}). c) CVs recorded during the electropolymerization of $\mathbf{3}(PF_6)_4$ (0.2 mM) by 15 potential cycles between −0.8 V and −1.8 V in 0.1 M Bu_4NClO_4/CH_3CN. The initial cycle is shown in red. d) CVs at 100 mV s^{-1} of the poly-$\mathbf{3}^{n+}$/ITO film obtained by 15, 30, and 45 potential cycles. ($\Gamma=4.4\times10^{-10}$, 1.4×10^{-9}, and 2.6×10^{-9} mol cm^{-2}, respectively). e) Absorption spectra and film picture of the poly-$\mathbf{3}^{n+}$/ITO film at different redox states ($\Gamma=5.0\times10^{-9}$ mol cm^{-2}).

decreased a little after six hours when the applied potential at +0.35 V was switched off. The retention time of poly-$\mathbf{3}^{4+}$ and poly-$\mathbf{3}^{5+}$ states are six hours and twenty minutes, respectively. This is long enough for a volatile memory.

To demonstrate the use of these films in flip-flop and flip-flap-flop memories, a relatively thin film ($\Gamma = 1.4 \times 10^{-9}$ mol cm^{-2}, about 15–20 nm thick) was used. A flip-flop memory only needs two input (In1 and In2) and two output (Out1 and Out1) signals. In this sense, three kind of flip-flop memories can be built from the poly-$\mathbf{3}^{n+}$ film by using any two redox states of poly-$\mathbf{3}^{3+}$, poly-$\mathbf{3}^{4+}$, and poly-$\mathbf{3}^{5+}$. Figure 5 shows ten repeated In1-read-In2-read cycles of flip-flop I (3+ and 4+ states are involved), flip-flop II (4+ and 5+ states), and flip-flop III (3+ and 5+ states). Taking flip-flop I as an example, when In2 at 0.75 V was applied, the Out1 at 1170 nm is high (the input and output strings are 0 1 and 1 0 respectively). On the contrary, when In1 at 0.35 V was applied, the Out2 at 1680 nm is high. When no inputs are applied, the output depends on the previous state. In each cycle, the electrochemical input was applied for 10 seconds. The response time is within a few seconds. This is followed by switching off the potential and reading the optical signals for 30 seconds. The signals essentially remain constant during the "read" process. The ON/OFF ratio is around 6 for both output signals. The other two flip-flops have similar performances.

The demonstrations of flip-flap-flop and ternary memory are shown in Figure 6. In this case, all three redox states (3+, 4+, and 5+) are involved. The logic circuit is composed of two parts.[7] The three electrochemical inputs (In1 at 0.35 V, In2 at 0.75 V, and In3 at 1.30 V) are first converted into three new input sequences (I_1, I_2, and I_3) with three OR gates. This is followed by three cross-coupled NOR gates to provide the memory and three optical outputs (Out1 at 750 nm, Out2 at 1170 nm, and Out3 at 1680 nm). The input and output signal changes of the poly-$\mathbf{3}^{n+}$/ITO film ($\Gamma = 1.4 \times 10^{-9}$ mol cm^{-2}, about 15–20 nm thick) during the ten repeated In1-read-In2-read-In3-read (10 seconds for input; 30 seconds for read) cycles are shown in Figure 6 a–d. During these processes, each output signal displays three levels of absorbance (0.041, 0.017, and 0.0097 for Out1; 0.077, 0.022, and 0.0033 for Out2; 0.035, 0.0075, and 0.0004 for Out3). However, the absorbance difference between the two lower-level signals of each output is small. For the flip-flap-flop memory, each output only needs two levels of signal (high for 1 and low for 0). The absorbance at 0.017 and 0.0097 of Out1 are thus both treated as the low output. A similar situation applies to the absorbance of 0.022 and 0.0033 of Out2 and 0.0075 and 0.0004 for Out3. When the input string is 0 0 1, 0 1 0, and 1 0 0, the output string is 1 0 0, 0 1 0, and 0 0 1, respectively (the upper section of Figure 6 f). When no potential is applied, the output is depending on the previous state. The order of the three input signals could be random. The input sequence in Figure 6 a and 6 c can also be treated as In2-In3-In1 or In3-In1-In2, in addition to In1-In2-In3. The film state depends on the last input applied. For the Out2 signal, a current spike is observed when the 5+ state is converted to the 3+ state. This indicates that the 5+ state was first reduced to the 4+ state, followed by a quick second reduction to the 3+ state.

As has been pointed out above, each output signal indeed displays three levels of absorbance. In this sense, the above electrochromic switching mimics a truly ternary memory with three inputs and three outputs and each output displays three levels of signal. The high, medium, and low absorbance of

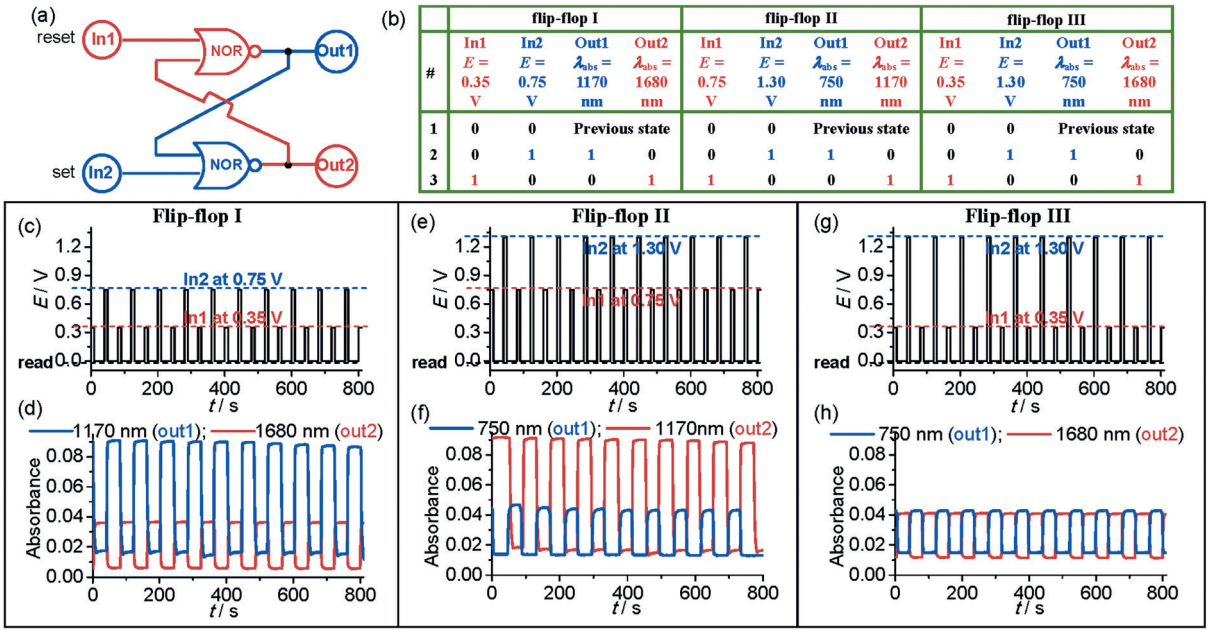

Figure 5. a) Logic circuit and b) truth tables of the set/reset flip-flop logic and the electrochemical input (c,e,g) and optical output (d,f,h) signal changes of flip-flop I (c,d), flip-flop II (e,f), and flip-flop III (g,h) based on the poly-$\mathbf{3}^{3+}$/ITO film ($\Gamma = 1.4 \times 10^{-9}$ mol cm^{-2}, about 15–20 nm thick). Ten repeated In1-read-In2-read cycles are shown. The electrochemical input was applied for 10 seconds, followed by switching off the potential and "reading" for 30 seconds.

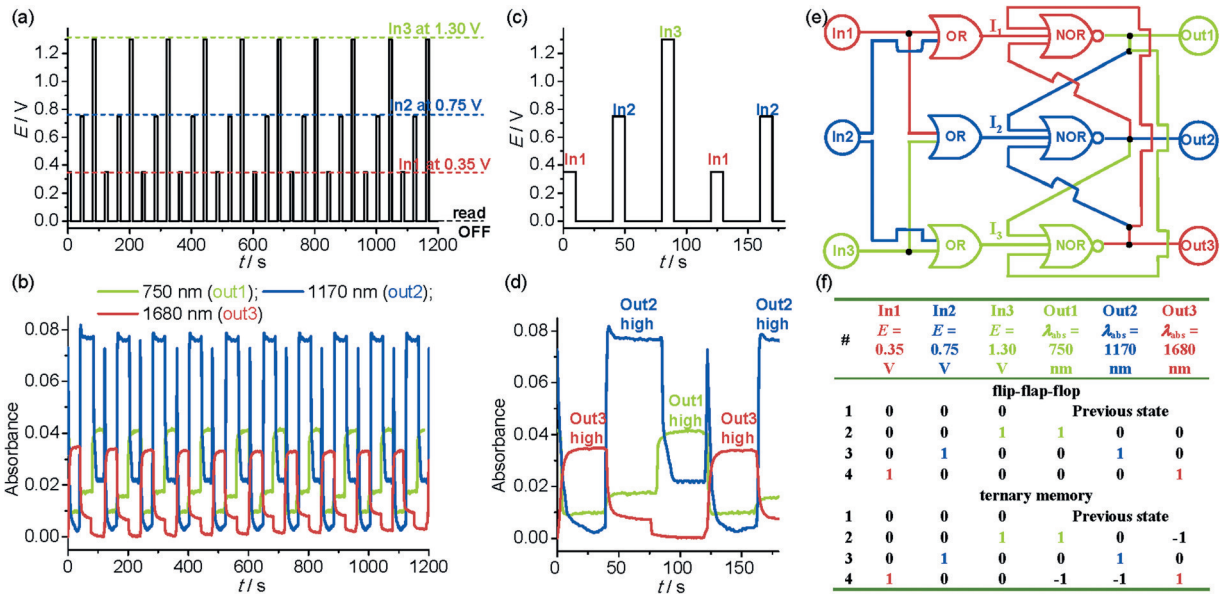

(f)

#	In1 E = 0.35 V	In2 E = 0.75 V	In3 E = 1.30 V	Out1 λ_{abs} = 750 nm	Out2 λ_{abs} = 1170 nm	Out3 λ_{abs} = 1680 nm
flip-flap-flop						
1	0	0	0	Previous state		
2	0	0	1	1	0	0
3	0	1	0	0	1	0
4	1	0	0	0	0	1
ternary memory						
1	0	0	0	Previous state		
2	0	0	1	1	0	-1
3	0	1	0	0	1	0
4	1	0	0	-1	-1	1

Figure 6. The input (a,c) and output (b,d) signal changes and truth tables (f) of the flip-flap-flop or ternary memory based on the poly-$\mathbf{3}^{3+}$/ITO film ($\Gamma = 1.4\times10^{-9}$ mol cm^{-2}, about 15–20 nm thick). (c) and (d) are partially enlarged plots of (a) and (b), respectively. e) The logic circuit of flip-flap-flop. Ten repeated In1-read-In2-read-In3-read cycles are shown.

each output is treated as the +1, 0, −1 level, respectively. The logic memory operates according to the lower section of the truth table shown in Figure 6 f. When In1 is applied, both Out1 and Out2 have medium absorbance whereas Out3 is high with an output string of −1 −1 1. When In2 or In3 is applied, the out string is 0 1 0 and 1 0 −1, respectively. The output signal ratio at three levels is 4.2/1.8/1 for Out1, 23/6.7/1 for Out2, and 85/18/1 for Out3, respectively. These high ratios ensure a low read error rate.

It should be noted that the circuit presented in Figure 6 is only an equivalent circuit. The three OR gates which convert the input states are just formal constructs and not real logic gates implemented in the molecular system. In addition, the logic operations of the present system is significantly different from the recently reported memories based on poly(3,4-ethylenedioxythiophene) (PEDOT) films.[46] PEDOT is essentially a bistable material. Multistate memories were achieved by using some intermediate potentials as input signals. However, all outputs are read at the same wavelength. The input potentials must be precisely controlled in order to decrease the error in reading the optical output. Our system features a truly four-state material and three optical outputs at different wavelengths. No stringent control of the input potentials is needed.

In conclusion, a new diruthenium complex with a redox-active amine bridge has been designed and synthesized. It shows multistate NIR electrochromism in solution and electropolymerized films. The most important feature is that it displays exclusive NIR absorbance at three different redox states. This feature, together with the good contrast ratio of each output and long retention time of each redox state, makes it a useful molecular platform for flip-flop, flip-flap-flop, and ternary memory. The materials used in this work have both advantages of sophisticated logic functions and simple film deposition. The film used in this study is around 15–20 nm thick. To increase the information density, a thinner film could also be used at the sacrifice of the signal/noise and ON/OFF ratio. In addition, the preparation and use of a monolayer film with suitable functional groups is also possible.[19] These works will be carried out and reported in due course.

Keywords: electrochemistry · memory · molecular device · molecular logic · ruthenium

How to cite: *Angew. Chem. Int. Ed.* **2015**, *54*, 9192–9197
Angew. Chem. **2015**, *127*, 9324–9329

[1] A. P. de Silva, H. Q. N. Gunaratne, C. P. McCoy, *Nature* **1993**, *361–366*, 277.
[2] K. Szaciłowski, *Chem. Rev.* **2008**, *108*, 3481.
[3] J. Andréasson, U. Pischel, *Chem. Soc. Rev.* **2010**, *39*, 174.
[4] A. P. de Silva, S. Uchiyama, *Nat. Nanotechnol.* **2007**, *2*, 399.
[5] G. de Ruiter, E. Tartakovsky, N. Oded, M. E. van der Boom, *Angew. Chem. Int. Ed.* **2010**, *49*, 169; *Angew. Chem.* **2010**, *122*, 173.
[6] P. Remón, M. Balter, S. Li, J. Andreasson, U. Pischel, *J. Am. Chem. Soc.* **2011**, *133*, 20742.
[7] G. de Ruiter, L. Motiei, J. Choudhury, N. Oded, M. E. van der Boom, *Angew. Chem. Int. Ed.* **2010**, *49*, 4780; *Angew. Chem.* **2010**, *122*, 4890.
[8] F. Meng, Y.-M. Hervault, Q. Shao, B. Hu, L. Norel, S. Rigaut, X. Chen, *Nat. Commun.* **2014**, *5*, 3023.
[9] C. Simão, M. Mas-Torrent, J. Casado-Montenegro, F. Otón, J. Veciana, C. Rovira, *J. Am. Chem. Soc.* **2011**, *133*, 13256.
[10] A. P. de Silva, *Nature* **2008**, *454*, 417.
[11] U. Pischel, *Angew. Chem. Int. Ed.* **2010**, *49*, 1356; *Angew. Chem.* **2010**, *122*, 1396.
[12] G. de Ruiter, M. E. van der Boom, *Acc. Chem. Res.* **2011**, *44*, 563.
[13] M. Mas-Torrent, C. Rovira, J. Veciana, *Adv. Mater.* **2013**, *25*, 462.

[14] Z. Liu, A. A. Yasseri, J. S. Lindsey, D. F. Bocian, *Science* **2003**, *302*, 1543.
[15] S. Sortino, S. Petralia, S. Conoci, S. D. Bella, *J. Am. Chem. Soc.* **2003**, *125*, 1122.
[16] C. Simão, M. Mas-Torrent, N. Crivillers, V. Lloveras, J. M. Artes, P. Gorostiza, J. Veciana, C. Rovira, *Nat. Chem.* **2011**, *3*, 359.
[17] K. Terada, K. Kanaizuka, V. M. Iyer, M. Sannodo, S. Saito, K. Kobayashi, M.-a. Haga, *Angew. Chem. Int. Ed.* **2011**, *50*, 6287; *Angew. Chem.* **2011**, *123*, 6411.
[18] G. de Ruiter, M. E. van der Boom, *Angew. Chem. Int. Ed.* **2012**, *51*, 8598; *Angew. Chem.* **2012**, *124*, 8726.
[19] B.-B. Cui, Y.-W. Zhong, J. Yao, *J. Am. Chem. Soc.* **2015**, *137*, 4058.
[20] A. Maier, A. R. Rabindranath, B. Tieke, *Adv. Mater.* **2009**, *21*, 959.
[21] R. Sakamoto, S. Katagiri, H. Maeda, H. Nishihara, *Coord. Chem. Rev.* **2013**, *257*, 1493.
[22] J. Poppenberg, S. Richter, C. H.-H. Traulsen, E. Darlatt, B. Baytekin, T. Heinrich, P. M. Deutinger, K. Huth, W. E. S. Unger, C. A. Schalley, *Chem. Sci.* **2013**, *4*, 3131.
[23] C. Musumeci, G. Zappala, N. Martsinovich, E. Orgiu, S. Schuster, S. Quici, M. Zharnikov, A. Troisi, A. Licciardello, P. Samori, *Adv. Mater.* **2014**, *26*, 1688.
[24] C. Friebe, M. D. Hager, A. Winter, U. S. Schubert, *Adv. Mater.* **2012**, *24*, 332.
[25] B.-B. Cui, C.-J. Yao, J. Yao, Y.-W. Zhong, *Chem. Sci.* **2014**, *5*, 932.
[26] Y.-W. Zhong, C.-J. Yao, H.-J. Nie, *Coord. Chem. Rev.* **2013**, *257*, 1357.
[27] A. P. Powell, C. W. Bielawski, A. H. Cowley, *J. Am. Chem. Soc.* **2010**, *132*, 10184.
[28] X.-Y. Chen, X. Yang, B. J. Holliday, *J. Am. Chem. Soc.* **2008**, *130*, 1546.
[29] C.-J. Yao, H.-J. Nie, W.-W. Yang, J.-Y. Shao, J. Yao, Y.-W. Zhong, *Chem. Eur. J.* **2014**, *20*, 17466.
[30] B.-B. Cui, Z. Mao, Y. Chen, Y.-W. Zhong, G. Yu, C. Zhan, J. Yao, *Chem. Sci.* **2015**, *6*, 1308.
[31] J. M. Spruell, A. Coskun, D. C. Friedman, R. S. Forgan, A. A. Sarjeant, A. Trabolsi, A. C. Fahrenbach, G. Barin, W. F. Paxton, S. K. Dey, M. A. Olson, D. Benitez, E. Tkatchouk, M. T. Colvin, R. Carmielli, S. T. Caldwell, G. M. Rosair, S. G. Hewage, F. Duclairoir, J. L. Seymour, A. M. Z. Slawin, W. A. Goddard III, M. R. Wasielewski, G. Cooke, J. F. Stoddart, *Nat. Chem.* **2010**, *2*, 870.
[32] A. Pron, P. Gawrys, M. Zagorska, D. Djurado, R. Demadrille, *Chem. Soc. Rev.* **2010**, *39*, 2577.
[33] G. Qian, Z. Y. Wang, *Chem. Asian J.* **2010**, *5*, 1006.
[34] W. Kaim, *Coord. Chem. Rev.* **2011**, *255*, 2503.
[35] C. M. Davis, K. Ohkubo, I.-T. Ho, Z. Zhang, M. Ishida, Y. Fang, V. M. Lynch, K. M. Kadish, J. L. Sessler, S. Fukuzumi, *Chem. Commun.* **2015**, *51*, 6757.
[36] T. Suzuki, T. Nakagawa, K. Ohkubo, S. Fukuzumi, Y. Matsuo, *Chem. Sci.* **2014**, *5*, 4888.
[37] J. García-Cañadas, A. P. Meacham, L. M. Peter, M. D. Ward, *Angew. Chem. Int. Ed.* **2003**, *42*, 3011; *Angew. Chem.* **2003**, *115*, 3119.
[38] Y. Qi, P. Desjardins, Z. Y. Wang, *J. Opt. A* **2002**, *4*, S273.
[39] C. Lambert, G. Nöll, *J. Am. Chem. Soc.* **1999**, *121*, 8434.
[40] K. Sreenath, T. G. Thomas, K. R. Gopidas, *Org. Lett.* **2011**, *13*, 1134.
[41] H. D. Abruña, P. Denisevich, M. Umaña, T. J. Meyer, R. W. Murray, *J. Am. Chem. Soc.* **1981**, *103*, 1.
[42] C.-J. Yao, Y.-W. Zhong, H.-J. Nie, H. D. Abruña, J. Yao, *J. Am. Chem. Soc.* **2011**, *133*, 20720.
[43] G. Sonmez, H. B. Sonmez, *J. Mater. Chem.* **2006**, *16*, 2473.
[44] A. L. Dyer, C. R. G. Grenier, J. R. Reynolds, *Adv. Funct. Mater.* **2007**, *17*, 1480.
[45] G. Qian, H. Abu, Z. Y. Wang, *J. Mater. Chem.* **2011**, *21*, 7678.
[46] G. de Ruiter, Y. H. Wijsboom, N. Oded, M. E. van der Boom, *ACS Appl. Mater. Interfaces* **2010**, *2*, 3578.

Received: May 20, 2015
Published online: July 3, 2015

